Uranyl Extraction by β-Diketonate Ligands to SC−CO_2: Theoretical Studies on the Effect of Ligand Fluorination and on the Synergistic Effect of TBP

Nicolas Galand and Georges Wipff*

Institut de Chimie, 4 rue B. Pascal, 67 000 Strasbourg, France

Received: May 24, 2004; In Final Form: August 25, 2004

We report theoretical investigations on the effect of H → F substitution in acetylacetonate ligands in order to understand why fluorination promotes the extraction of uranyl to supercritical CO_2 with a marked synergistic effect of tri-*n*-butyl phosphate "TBP". The neutral **L**H and deprotonated $\mathbf{L}^-$ forms of the ligand, and the uranyl complexes $UO_2\mathbf{L}_2$ and $UO_2\mathbf{L}_2S$ (S = H_2O versus trimethyl phosphate "TMP" which mimics TBP) are studied by quantum mechanics (QM) in the gas phase, whereas the ligands **L**H and their $UO_2\mathbf{L}_2$ and $UO_2\mathbf{L}_2S$ complexes are studied by molecular dynamics (MD) in SC−CO_2 solution as well as at a CO_2−water interface. Several effects are found to favor F ligands over the H ligands. (i) First, intrinsically (in the gas phase), the complexation reaction 2 **L**H + UO_2^{2+} → $UO_2\mathbf{L}_2$ is more exothermic for the F ligands, mainly due to their higher acidity, compared to the H ligands. (ii) The unsaturated $UO_2\mathbf{L}_2$ complexes with F ligands bind more strongly TMP than H_2O, thus preferentially leading to the $UO_2\mathbf{L}_2$(TMP) complex, more hydrophobic than $UO_2\mathbf{L}_2(H_2O)$. (iii) Molecular dynamics simulations of SC−CO_2 solutions show that the F ligands and their $UO_2\mathbf{L}_2$ and $UO_2\mathbf{L}_2S$ complexes are better solvated than their H analogues, and that the $UO_2\mathbf{L}_2$(TBP) complex with F ligands is the most CO_2-philic. (*iv*) Concentrated solutions of $UO_2\mathbf{L}_2$(TBP) complexes at the CO_2−water interface display an equilibrium between adsorbed and extracted species, and the proportion of extracted species is larger with F− than with H− ligands, in agreement with experimental observations. Thus, TBP plays a dual synergistic role: its co-complexation by $UO_2\mathbf{L}_2$ yields a hydrophobic and CO_2-philic complex suitable for extraction, whereas TBP in excess at the interface facilitates the migration of the complex to the supercritical phase.

Introduction

Supercritical fluid extraction to CO_2 "SC−CO_2" is emerging as a promising "green alternative" to extract and separate metal ions from an aqueous phase, presenting the major advantages of being based on a nontoxic, environmentally acceptable, and cheap solvent with a low critical temperature and a moderate critical pressure.[1] The effectiveness of the technique depends largely on the choice of the ligands and Wai et al.[2,3] early noticed that the solubility of metal dicarbamates in SC−CO_2 is greatly enhanced upon fluorination of the ligand. Since, many extraction systems have been reported, involving chelating agents, such as dithiocarbamates, thenoyltrifluoacetone, phosphoryl-containing ligands, macrocylic compounds, or fluorinated surfactants. For reviews, see, e.g. refs 1,4−6. In this paper, we focus on β-diketones (Figure 1) which represent an important class of chelating acidic ligands which promote the metal extraction to SC−CO_2.[7] The first example concerns the Fe^{3+} complexation to SC−CO_2 by acetylacetonate ligands (hereafter noted AA^-; see Figure 1), forming $Fe(AA)_3$ complexes.[8] The report of trivalent lanthanide and of uranyl cation extraction to SC−CO_2 by the fluorinated β-diketones FOD (2,2-dimethyl-6,6,7,7,8,8)-heptafluoro-3,5-octanedione) or FAH (1,1,1,6,6,6,-hexafluoro-pentane-2,2,-dione) opened important perspectives in the field of nuclear waste partitioning based on "green technology".[9] Further developments involve the extraction of these ions by a mixture of fluorinated ligands and synergistic ligands "S" like methanol, tributyl phosphate (TBP), tributylphosphine oxide (TBPO), or trioctylphoshine oxide (TOPO).[10−12] The formation of adducts with the neutral donors S greatly improves the solubility of the complex in the supercritical phase and its detection sensitivity.[11,13] We thus decided to investigate by theoretical simulations the uranyl extraction by acetylacetonate

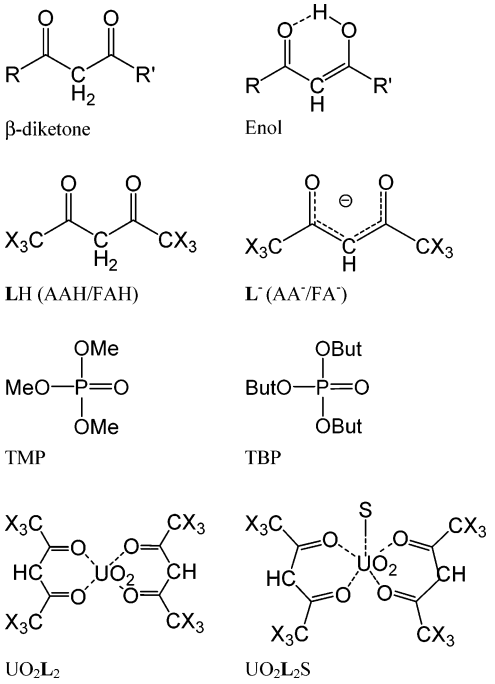

Figure 1. Simulated neutral **L**H and deprotonated $\mathbf{L}^-$ ligands, TMP and TBP, and their uranyl complexes.

* To whom correspondence should be addressed. E-mail: wipff@chimie.u-strasbg.fr.

10.1021/jp047761z CCC: $30.25
Published on Web 12/09/2004

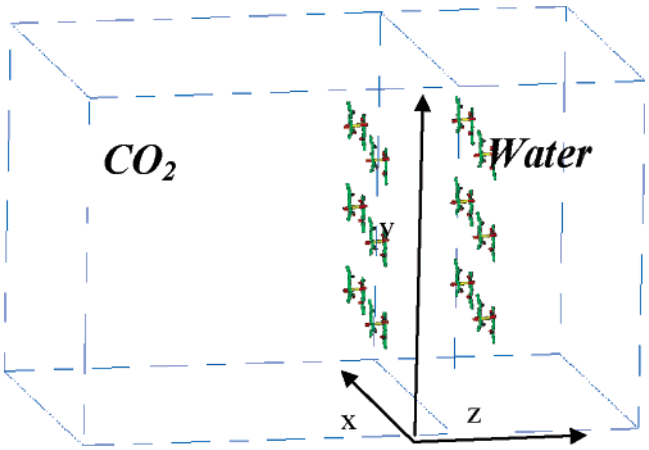

Figure 2. Schematic representation of the CO_2/water interface with a grid of 12 $UO_2(AA)_2$ complexes.

ligands (AA^-) and their perfluoro analogues (FA^-) to SC−CO_2, aiming at understanding (i) why the ligand fluorination favors the extraction and (ii) the synergistic effect of TBP molecules. For this purpose, two complementary approaches are used. First, the complexation of H versus F ligands by uranyl is investigated in the gas phase by quantum mechanical methods. The formation of four-coordinated $UO_2\mathbf{L}_2$ and of five-coordinated UO_2L_2S uranyl complexes will be compared with $\mathbf{L}^- = AA^-$ versus FA^- ligands and S = H_2O versus TBP (Figure 1). We want to determine whether fluorination intrinsically favors the ligand complexation and to compare the affinity of the unsaturated $UO_2\mathbf{L}_2$ complex for H_2O versus TBP, which has a great influence on the hydrophilic/hydrophobic character and extractability of the complex. We then simulate by molecular dynamics the H versus F ligands and their complexes in a pure SC−CO_2 solution, as well as at a SC−CO_2/ water interface, to investigate the effect of ligand fluorination and of TBP co-complexation on the solvation and interfacial behavior of the complexes. The free ligands and their complexes are expected to be surface active and to concentrate in the interfacial region.[14−19] It will thus be particularly interesting to gain microscopic insights into the extraction process and to see to which extent the ligand fluorination and the TBP synergistic effect will promote the extraction of the complexes to the supercritical phase.

Methods

Quantum Mechanical Calculations in the Gas Phase. The ligands and their complexes were fully optimized by quantum mechanical calculations at the Hartree−Fock (HF) and density functional (DFT with the B3LYP functional) levels of theory, using the Gaussian 98 software.[20] The H, C, N, O, and F atoms were described by the 6-31G* basis set. For uranium, we used a relativistic large core effective core potential (ECP) of the Los Alamos group with 78 electrons in the core and a [3s,3p,-2d,2f] contracted valence basis set.[21] This level of theory is sufficient to gain insights into energy and structural features of ligand binding to uranyl.[22,23] Additional insights into correlation effects were obtained by MP2//HF and MP2//DFT single-point calculations on HF and on DFT optimized structures. There are several DFT studies on uranyl complexes[24−28] as well as studies based on HF + perturbation calculations.[29−32] See also ref 33 for a discussion of recent developments in computational actinide chemistry. Another issue concerns the uranium representation and tests on uranyl complexes using the Stuttgart ECPs with 60 electrons in the core[34,35] yielded similar structures and ligand binding energies as those obtained with the large ECP we used.[36] Some tests with this smaller ECP have been repeated here for key systems. The protonation and complexation energies were corrected from basis set superposition errors (BSSE) using the counterpoise method.[37] Insights into the electron distribution were obtained from the analysis of Mulliken charges.

Molecular Dynamics (MD) Simulations in CO_2 Solution and at the SC−CO_2/Water Interface

Empirical Representation of the Potential Energy. The MD simulations were performed with the modified AMBER7.0 software[38] where the potential energy is described by a sum of bond, angle and dihedral deformation energies, and pair wise additive 1−6−12 (electrostatic + van der Waals) interactions between nonbonded atoms

$$U = \Sigma_{\text{bonds}} K_r (r - r_{eq})^2 + \Sigma_{\text{angles}} K_\theta (\theta - \theta_{eq})^2 + \Sigma_{\text{dihedrals}} \Sigma_n V_n (1 + \cos n\phi) + \Sigma_{i<j} [q_i q_j / R_{ij} - 2\epsilon_{ij} (R_{ij}^*/R_{ij})^6 + \epsilon_{ij} (R_{ij}^*/R_{ij})^{12}]$$

The charges of the free **L**H and $\mathbf{L}^-$ ligands were derived from ESP potentials calculated with the 6-31G* basis set. For their uranyl complexes, we preferred to use Mulliken charges (from DFT//DFT calculations) which somewhat reflect the electronic reorganization (charge transfer and polarization effects) in systems with buried atoms than ESP charges.[39] They are given with the AMBER atom types in Figure S1. Tests with ESP Merz−Kollman charges (from DFT//DFT calculations) were also performed for comparison. The van der Waals parameters of uranium ($R^*_U = 1.58$ Å, $\epsilon_U = 0.4$ kcal/mol) are from ref 40, and those of fluorine ($R^*_F = 1.75$ Å, $\epsilon_F = 0.061$ kcal/mol) were from Kollman et al.[41] The solvent models were derived from studies on the liquid properties. CO_2 was represented by the three-points model of Murthy et al.[42] (charges $q_C = 0.596$, $q_O = -0.298$ e and van der Waals parameters $R^*_O = 1.692$, $R^*_C = 1.563$ Å and $\epsilon_O = 0.165$, $\epsilon_C = 0.058$ kcal/mol) and water was represented with the TIP3P model.[43] All O−H and C−H bonds and the C═O bonds of CO_2 were constrained with SHAKE, using a time step of 2 fs. The intramolecular electrostatic and van der Waals 1···4 interactions were scaled down by a factor 2.0, as recommend by Cornell et al.[44] Nonbonded interactions were calculated with an atom-based cutoff of 12 Å, in conjunction with the EWALD summation method (PME approximation)[45] to account for long-range Coulombic interactions. The "non-bonded" pair lists were updated every step.

Solutions and Dynamics. The CO_2 solutions were prepared by immersing the solute in a cubic CO_2 box of ≈36 Å length, containing 500 CO_2 molecules. The corresponding density is 0.80, which is above the critical density (0.47 g cm^{-3} at 304 K) and close to the experimental density of 0.79 g cm^{-3} at 345 K and a pressure of 30 Mpa.[46] The solutions were represented with 3D periodic boundary conditions. The CO_2−water interface has been built starting with adjacent boxes of CO_2 and pure water (see Figure 2). The characteristics of the simulated solutions are given in Table 1.

After energy minimization, MD in solution was run at 350 K and constant volume, first for 50 ps with the solute frozen (in order to relax the solvent molecules), followed by unconstrained dynamics. The temperature was monitored by coupling the system to a thermal bath at the reference temperature with a relaxation time of 0.2 ps using the Berendsen algorithm.[47]

Analysis of Results. The trajectories were saved every 0.5 ps and analyzed. An energy component analysis was performed in terms of pair wise additive contributions of the solvent and the solute, using a 17 Å cutoff with a reaction field "RF"

TABLE 1: Characteristics of the Simulated CO_2/Water Interfacial Systems: Box Size, Number of Solvent Molecules and Simulated Time

solute	box size (Å^3) V_x* V_y* ($V_{z\text{-}CO_2}$ + $V_{z\text{-}Wat}$)	N_{CO_2}	N_{H_2O}	time (ns)
96 AAH enol	38*38*(37 + 28)	500	1000	2
96 FAH enol	39*38*(37 + 28)	500	1000	2
12 UO_2^{2+}; 24 AA^-	40*39*(36 + 36)	501	1688	2
12 UO_2^{2+}; 24 FA^-	40*39*(36 +38)	501	1800	2
12 $UO_2(AA)_2$	49*50*(55 + 25)	1468	2057	1.5
12 $UO_2(FA)_2$	50*51*(55 + 25)	1536	2061	1.5
12 $UO_2(AA)_2$(TBP)	51*53*(55 + 25)	1396	1872	1.5
12 $UO_2(FA)_2$(TBP)	51*53*(55 + 25)	1528	2025	1.5
12 $UO_2(AA)_2$(TBP) + 60 TBP	53*53*(55 + 25)	1400	1800	2
12 $UO_2(FA)_2$(TBP) + 60 TBP	53*53*(55 + 26)	1400	1900	2

TABLE 2: Calculated Energies (kcal/mol) of Reactions 1−12, as Defined in the Text

energy	HF	DFT	MP2//HF	MP2//DFT
ΔE_1 X = H	370.6	367.3	364.7	365.2
X = F	335.1	334.9	327.8	330.9
ΔE_2 X = H	−571.7	−591.1	−597.5	−593.2
X = F	−506.0	−528.1	−532.1	−528.1
ΔE_3 X = H	169.3	143.5	132.0	137.2
X = F	164.1	141.7	123.5	133.7
ΔE_4	−5.2	−1.8	−8.5	−3.5
ΔE_4[a]	−4.9	−2.4		
ΔE_5	−12.9	−10.8	−14.2	−12.9
ΔE_6	−19.3	−16.5	−17.1	−16.3
ΔE_7	−15.5	−9.8	−20.2	−17.8
ΔE_8	−28.0	−19.4	−27.6	−27.1
ΔE_9	−17.4	−12.9	−20.4	−14.2
ΔE_{10}	−10.8	−6.2	−13.4	−8.7
ΔE_{11}	−2.2	+1.9	−3.1	−4.8
ΔE_{12}	−8.7	−4.8	−9.5	−9.7

[a] Small ECP on the U atom.

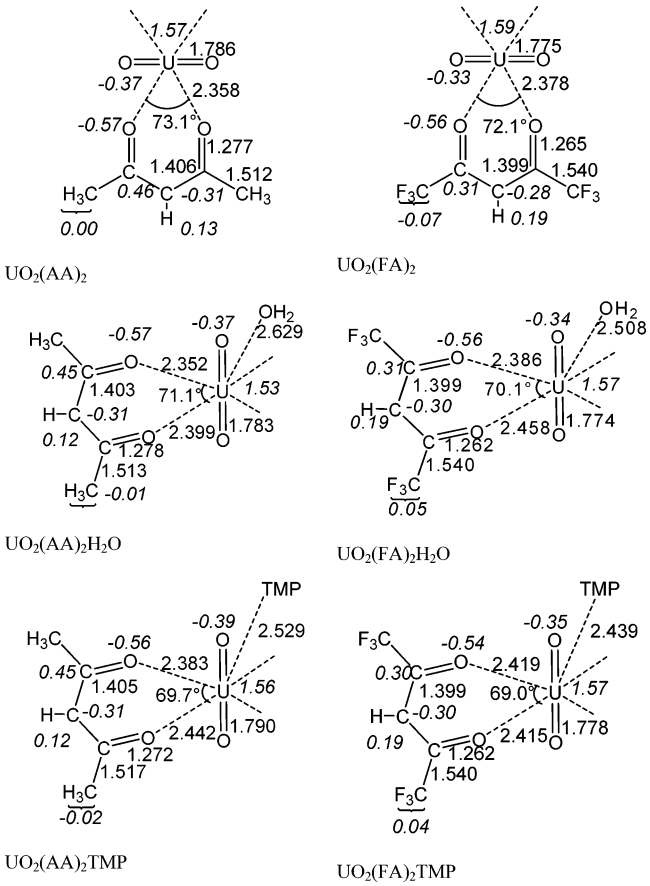

Figure 3. DFT optimized distances (in Å) of the $UO_2(AA)_2$, $UO_2(FA)_2$ complexes and their adducts with TMP and H_2O. Mulliken charges (in italics). See also Tables 3 and 4.

correction.[48] The distribution of the solutes with respect to the interface has been characterized from the average density curves as a function of *z* direction (perpendicular to the interface), calculated during the last 0.2 ns. The *z* position of the interface was dynamically defined by the intersection of the CO_2 and water density curves, and the proportion of species "at the interface" was integrated within ±8 Å from the interface, which corresponds to the distance after which the solvent densities are close to their "bulk" values. The instantaneous CO_2 surface at the interface was defined by the z_{max} coordinates of CO_2 molecules which remain in contact with the bulk CO_2, thus excluding isolated CO_2 molecules. The water surface is defined similarly.

Results

We first analyze the interactions of H- versus F-diketonate ligands with the uranyl cation in the gas phase. This is followed by the analysis of solvation of uranyl complexes with H/F ligands in CO_2 solution and their distribution at the CO_2−water interface.

I. Interactions between H- / F-*β*-Diketonates and the Uranyl Cation in the Gas Phase. The total energies of the optimized species (HF, DFT, and MP2 levels) are given in Table S1. Table 2 contains the energy results of reactions 1−12. The main structural and electronic results are summarized in Tables 3 (for $UO_2\mathbf{L}_2$ complexes) and 4 (for $UO_2\mathbf{L}_2$S complexes) and shown in Figure 3. Unless otherwise specified, the numbers given below correspond to the DFT calculations. The latter are a priori more satisfactory as they account for the electron correlation energy. In the metal complexes, the optimized metal−ligand distances are also shorter with the DFT than with HF methods, thus generally leading to a better agreement between calculated and experimental solid-state structures.[36] In the present study, HF, DFT, and MP2 methods yield similar conclusions as far as the effect of ligand fluorination is concerned.

Free AAH and FAH Ligands: Tautomerism and Basicity. The studied **L**H ligands display in principle keto/enol tautomerism and, for each state, several possible conformers.[49] In the gas phase, however, they prefer the planar *cis*-enolic form, further stabilized by internal hydrogen bonding. This is supported by gas-phase electron diffraction studies on AAH [50−52] and FAH,[53] by IR-spectroscopic data on AAH,[54] as well as by a quantum mechanical study in which the different forms of the enol and the diketone were compared.[55] This cyclic *cis*-2-enol was found to be 1.1 kcal/mol more stable than the trans diketone form (MP2 calculations with a D95** basis set) and to display an asymmetrical bridging proton coordination. A similar structure is found in the crystalline state for AAH itself at low temperature[56] and in a series of *β*-diketone fragments.[57] The structure of the enol forms of *β*-diketones AAH and FAH has also been investigated by QM calculations at the HF and correlated MP2 to MP4 levels.[58] NMR data indicate that the fluorinated diketones are almost exclusively in the enol form under the high pressure and temperature conditions relevant to supercritical fluid extraction.[59] According to our calculations on AAH and FAH, the *cis*-enol is more stable than the *trans*-diketone form, by 3.3 and 5.5 kcal/mol, respectively. This is why the planar *cis*-enol form was taken as the reference state for the free AAH and FAH neutral ligands.

For the deprotonated AA^- and FA^- states, the cis form, suitable for complexation, was also chosen as a reference. According to HF and DFT calculations, FA^- cis is more stable FA^- trans (by 6.2 and 6.4 kcal/mol, respectively), whereas AA^- cis is less stable than AA^- trans (by 4.5 and 3.4 kcal.mol, respectively). Thus, a positive effect of fluorination is to favor the cis form of the diketonate ligands, thus avoiding the energy price to be paid for trans to cis rearrangement upon complexation.[60]

$$\mathbf{L}H \rightarrow \mathbf{L}^- + H^+ \qquad (1)$$

Insights into the effect of ligand fluorination on its intrinsic basicity were obtained from the deprotonation reaction 1, comparing AAH versus FAH "acids". The results (Table 2) show that is less endothermic (by 36 kcal/mol at the HF level and 32 kcal/mol at the DFT level) with FAH than with AAH. We are not aware of experimental data in the gas phase, but the trend is consistent with lower pK_a of FAH, compared to AAH in water (4.5 and 8.7, respectively),[61] as well as with the larger acidity of the 1,1,1-trifluoroacetylacetone, compared to acetylacetone AAH in the gas phase ($\Delta G° = 15.6$ kcal/mol).[62] The electron withdrawing effect of fluorine can be illustrated by the change of q_O carbonyl charges which become less negative upon ligand fluorination (from -0.45 to -0.34 e for the diketones, from -0.52 to -0.47 e for the enols, and from -0.55 to -0.51 e for the deprotonated ligands; see Tables S2 and S3). Structural characteristics of the $\mathbf{L}^-$ and $\mathbf{L}$H ligands can be found in Tables S2 to S4, showing weakened internal hydrogen bonds in the LH enols (vide infra) and strengthened carbonyl bonds in $\mathbf{L}$H diketones and in $\mathbf{L}^-$ diketonates upon fluorination.

Formation of Four-Coordinated Uranyl Complexes. The decrease of carbonyl oxygens basicity upon fluorination is expected to lower the ligand affinity for uranyl

$$UO_2^{2+} + 2\,\mathbf{L}^- \rightarrow UO_2\mathbf{L}_2 \qquad (2)$$

This is indeed observed upon formation of $UO_2\mathbf{L}_2$ complexes (eq 2). The anionic AA^- and FA^- ligands display a strong affinity for uranyl (Table 2) and complexation is much less exothermic with FA^- than with AA^-, by 66 kcal /mol (HF level) and 63 kcal /mol (DFT level). Both optimized structures display a D_{2h} type symmetry with four equal $U-O_L$ equatorial bonds (Figure 3 and Table 3), and the lower stability of the $UO_2(FA)_2$ complex, compared to $UO_2(AA)_2$, is visible in the $U-O_{FA}$ bonds that are 0.02 Å longer than the $U-O_{AA}$ bonds (2.38 and 2.36 Å, respectively). The weaker coordination of the F ligand is also reflected by a stronger and shorter U═O bond in the F complex than in the H complex (1.78 and 1.79 Å, respectively). The intra-ligand O···O distances are similar in the F and H complexes (2.80 and 2.81 Å, respectively). They are shorter by only 0.28 and 0.20 Å, respectively, compared to the corresponding free cis ligands, indicating they undergo minor structural reorganization upon complexation.

The weaker complexation of FA^-, compared to AA^- ligands is also reflected by the electron distribution (Table 3) which indicates less ligand-to-uranyl charge transfer in the F complex ($q_{UO2} = +0.91$ e) than in the H complex ($q_{UO2} = +0.82$ e). Each complexed FA^- ligand is thus more negatively charged (by ≈ 0.05 e) than an AA^- ligand. The carbonyl groups are also less polar in FA^- (charges are $O^{-0.56}-C^{0.31}$) than in AA^- complexed ligands ($O^{-0.57}-C^{0.45}$).

Reaction (2) models a complexation process starting with diketonate anions. If the reaction is carried out from neutral $\mathbf{L}$H ligands,[6,63,64] the conclusion may differ, are this reaction formally involves deprotonation of $\mathbf{L}$H to $\mathbf{L}^-$ (which favors F ligands), followed by the complexation of $\mathbf{L}^-$ (which favors H ligands). Which of these effects will dominate is examined via the reaction 3:

$$UO_2^{2+} + 2\mathbf{L}H \rightarrow UO_2\mathbf{L}_2 + 2\,H^+ \qquad (3)$$

The resulting energies ΔE_3 (Table 2) show that complexation of the F ligands is favored, at the HF, DFT, //HF, and MP2// DFT computational levels (by 5.2, 1.8, 8.5, and 3.5 kcal/mol, respectively). The same conclusion is obtained from an isodesmic reaction 4

$$UO_2(AA)_2 + 2\,FAH \rightarrow UO_2(FA)_2 + 2\,AAH \qquad (4)$$

The calculated ΔE_4 energy is negative (from -1.8 to -8.5 kcal/mol, depending on the computational level), showing the F complex is favored over the H complex, and this conclusion is confirmed by QM optimizations of the complexes using a smaller ECP on uranium:[34,35] $\Delta E_4 = -4.9$ and -2.4 kcal/mol at the HF and DFT levels, respectively. The higher enthalpic stability of the F complex thus results from the compromise between antagonistic acidity and complexation properties.

Formation of Five-Coordinated Uranyl Complexes. Uranyl generally coordinates five to six oxygens in its equatorial plane, and in the solid-state structures of uranyl diketonate complexes recorded in the Cambridge Structural Data Base,[65] uranyl is coordinated to an additional ligand S, like H_2O in the $UO_2(AA)_2(H_2O)$ complex,[66] or the TBP molecule in the $UO_2(FA)_2$(TBP) complex.[67] Analogues are found with S = carbonyl, phosphoryl, alcohol, or nitrogen containing ligands.[68] Such adduct formation has also been observed in classical [69] as well as in supercritical solvent extraction of uranyl with β-diketones and organophosphorus reagents.[10,11,70] Similar co-complexation of neutral oxygen or nitrogen donors S is observed in solid state structures of $M\mathbf{L}_3$ β-diketonate complexes of trivalent (e.g., M = lanthanide, yttrium, scandium) metals. As the ligand binding strength is expected to increase with its basicity (as indicated

TABLE 3: Main Structural and Electronic Features of the UO_2L_2 Complexes[a]

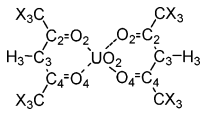

		$UO_2(AA)_2$		$UO_2(FA)_2$	
		HF	DFT	HF	DFT
distance (Å)	$U-O_U$	1.716	1.786	1.707	1.775
	$U-O_2$	2.378	2.358	2.404	2.378
	$C-C_2$	1.507	1.512	1.531	1.540
	C_2-C_3	1.399	1.406	1.392	1.399
	C_2-O_2	1.254	1.277	1.240	1.238
	$O_2\cdots O_4$	2.815	2.810	2.789	2.802
angle (°)	$O_2-C_2-C_3$	125	125	128	124
	O_2-C_2-C	115	116	113	114
	$C_2-C_3-C_4$	125	125	122	122
	O_2-U-O_4	73	73	71	72
Mulliken charges (e)	U	2.320	1.566	2.314	1.588
	O_U	−0.480	−0.374	−0.441	−0.334
	UO_2	1.360	0.818	1.432	0.920
	L	−0.680	−0.409	−0.716	−0.460
	O_2	−0.831	−0.570	−0.808	−0.555
	C_2	0.635	0.456	0.455	0.306
	C_3	−0.532	−0.310	−0.497	−0.290
	H_3	0.192	0.129	0.275	0.194
	C	−0.568	−0.528	1.303	0.892
	X	0.198	0.176	−0.399	−0.275
	CX_3	0.026	0.000	0.106	−0.067

[a] The ESP charges are given in Table S6.

by its "donor number" DN [71]), TBP (DN = 24 kcal/mol) should bind more strongly than H_2O (DN = 18 kcal/mol) to uranyl, but to our knowledge, there is no direct comparison of the studied F versus H complexes.

We thus first modeled the complexation of H_2O versus TBP to $UO_2\mathbf{L}_2$. For computer-time-saving purposes, and in order to avoid the issues of multiple conformations of the butyl chains, TBP was modeled by TMP (*tri*-methoxyphosphate $(MeO)_3P{=}O$)

$$UO_2(AA)_2 + H_2O \rightarrow UO_2(AA)_2(H_2O) \quad (5)$$

$$UO_2(FA)_2 + H_2O \rightarrow UO_2(FA)_2(H_2O) \quad (6)$$

$$UO_2(AA)_2 + TMP \rightarrow UO_2(AA)_2(TMP) \quad (7)$$

$$UO_2(FA)_2 + TMP \rightarrow UO_2(FA)_2(TMP) \quad (8)$$

The energies ΔE_5 to ΔE_8 of reactions 5−8 are clearly exothermic. At the HF, DFT, MP2//HF, and MP2//DFT levels of theory, they range from −13 to −28, − 10 to −19, −14 to −28, and −13 to −27 kcal/mol, respectively (Table 2), showing that the unsaturated $UO_2\mathbf{L}_2$ complexes can further bind a monodentate ligand, leading to a five coordinated uranyl. The most important result concerns the role of ligand fluorination on the affinity for H_2O versus TMP. The fluorinated $UO_2(FA)_2$ complex indeed clearly prefers TMP to H_2O, at the HF and DFT levels of theory (by ≈ 9 and 3 kcal/mol, respectively), as well as at the MP2//HF and MP2//DFT levels (by ≈ 10 and 11 kcal/mol, respectively). This is a crucial feature in the context of liquid−liquid extraction because the $UO_2(FA)_2(TMP)$ complex is more hydrophobic and should be more amenable to extraction than the hydrated $UO_2(FA)_2(H_2O)$ complex.

For the $UO_2(AA)_2$ H complex, the conclusion is less clear and depends on the level of calculations. The complex slightly prefers TMP to H_2O at the HF, MP2//HF, and HF//DFT levels (by ≈ 3, 6 and 5 kcal/mol, respectively), whereas the reverse is observed (by 1 kcal/mol) at the DFT level. We notice that these numbers are smaller than for the F complex, indicating no clear preference to select an extra ligand. Thus, some H complexes may further bind water and are thus more hydrophilic than their F analogues are, which is deleterious as far as liquid−liquid extraction is concerned.

Another comparison of the five-coordinated complexes can be made via the reactions 9 and 10 in which H ligands are exchanged with F ligands

$$UO_2(AA)_2(TMP) + 2\ FAH \rightarrow UO_2(FA)_2(TMP) + 2\ AAH \quad (9)$$

$$UO_2(AA)_2(H_2O) + 2\ FAH \rightarrow UO_2(FA)_2(H_2O) + 2\ AAH \quad (10)$$

The two reactions are exothermic (≈ −6 to −13 kcal/mol) which confirms that, in the presence of an additional H_2O or phosphoryl-containing ligand, F ligands still bind more strongly than their H analogues. An important point is that, at both HF and DFT levels, the preference is more pronounced with TMP (by −17 and −13 kcal/mol, respectively) than with H_2O (by −11 and −6 kcal/mol, respectively) as the extra ligand. MP2//HF and MP2//DFT calculations yield the same conclusion (see Table 2). Thus, the effect of fluorination should be most effective in a relatively "dry" medium rich in TBP. This is in fact the case of SC−CO_2 solution of TBP and diketone ligands used in liquid−liquid extraction

$$UO_2(AA)_2(H_2O) + TMP \rightarrow UO_2(AA)_2(TMP) + H_2O \quad (11)$$

$$UO_2(FA)_2(H_2O) + TMP \rightarrow UO_2(FA)_2(TMP) + H_2O \quad (12)$$

The dual effect of TMP binding and ligand fluorination is also demonstrated by reactions 11 and 12 in which H_2O is exchanged with TBP. Again, the F complex clearly prefers TMP to H_2O, thus leading to a hydrophobic and CO_2-philic $UO_2(FA)_2(TMP)$ complex (ΔE_{12} ranges from −5 to −10 kcal/mol, depending on the computational level; Table 2). In the case of the H complex, no firm conclusion can be drawn, as ΔE_{11} is smaller in magnitude than ΔE_{12}, and is positive (+2 kcal/mol) at the DFT level, but negative at the HF, MP2//HF, and MP2//DFT levels (−2, −3 and −5 kcal/mol, respectively). We note that the lack of clear-cut preference for H_2O versus TMP concerns the H complex, which is in fact less extracted than the F complex to CO_2.

Why Does TMP Bind More Strongly to $UO_2(FA)_2$ than to the $UO_2(AA)_2$ Complex? When an additional ligand S binds to the unsaturated $UO_2\mathbf{L}_2$ complex, there is compromise to be found between a strong coordination of S and of **L**, due to the resulting steric strain in the first coordination shell. The tighter is the binding of **L**, the weaker is the U−O_S bond, and vice versa. The effect is clearly visible in the optimized structures of the complexes (see Table 4 and Figure 3). TMP, more basic than H_2O, makes stronger and shorter bonds in all complexes. The U−O_{TMP} distances (2.53 Å in the $UO_2(AA)_2(TMP)$ complex and 2.44 Å in $UO_2(FA)_2(TMP)$) are ≈0.1 Å shorter than the U−O_{H2O} distances (2.63 Å in the $UO_2(AA)_2(H_2O)$ complex and 2.51 Å in $UO_2(FA)_2(H_2O)$). The preference for TMP over H_2O is more pronounced with the F than for the H complex. This is because the U−O_{FA} bonds are somewhat weaker and more easily stretchable than the U−O_{AA} bonds are, thus allowing for a tighter binding of the TMP ligand. As a result, the U−O_{TMP} bond shortens by 0.08 Å upon ligand fluorination in the $UO_2\mathbf{L}_2$-(TMP) complexes. A similar shortening of the U−O_{H2O} distances (0.06 Å) is found in the hydrated $UO_2\mathbf{L}_2(H_2O)$ complexes.[72] Changes in the internal U═O bond of uranyl also mirror the changes in metal−ligand strength: for a given H_2O or TMP ligand, U═O shortens by ≈ 0.01 Å upon ligand fluorination, and for a given diketonate ligand, U═O lengthens by ≈ 0.005 Å when H_2O is displaced by TMP.

Thus, to summarize this section, according to QM calculations in the gas phase, fluorinated FAH diketones form stronger complexes with uranyl than their H analogues AAH do, be uranyl tetra- or pentacoordinated. In addition, when compared to its H analogue $UO_2(AA)_2$, the fluorinated $UO_2(FA)_2$ complex displays a stronger affinity for a phosphoryl-containing ligand than for water. It is certainly not coincidental that in the X-ray structure of the uranyl complexes, the fifth site is occupied by TBP with the F-diketonate ligand,[67] and by an H_2O molecule with the H-diketonate ligands.[66] This is fully consistent with our calculated results.

II. Free Ligands and Their Uranyl Complexes in CO_2 Solution. Simulation of the free ligands and of their complexes [73] in pure SC−CO_2 liquid show that these species display attractive interactions with the solvent which are larger with the F than with the H ligands (see energy results in Tables 5 and S5).

This is first observed with the two tautomeric forms of the free ligands: FAH interacts more than AAH with CO_2 (−13.8 versus −13.0 kcal/mol, respectively, for the diketone forms, and −13.4 versus −10.9 kcal/mol, respectively, for the enol

TABLE 4: Main Structural and Electronic Features of the UO_2L_2S Complexes[a]

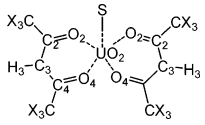

		$UO_2(AA)_2(H_2O)$		$UO_2(FA)_2(H_2O)$		$UO_2(AA)_2(TMP)$		$UO_2(FA)_2(TMP)$	
		HF	DFT	HF	DFT	HF	DFT	HF	DFT
distance (Å)	$U-O_U$	1.717	1.783	1.708	1.774	1.723	1.790	1.713	1.778
	$U-O_2$	2.445	2.399	2.460	2.458	2.459	2.442	2.472	2.415
	$U-O_4$	2.390	2.352	2.425	2.386	2.414	2.383	2.450	2.419
	$U-O_S$	2.589	2.629	2.561	2.508	2.495	2.529	2.438	2.439
	C_1-C_2	1.508	1.513	1.532	1.540	1.509	1.517	1.531	1.540
	C_2-C_3	1.401	1.403	1.395	1.399	1.402	1.405	1.389	1.402
	C_2-O_2	1.251	1.278	1.237	1.262	1.248	1.272	1.254	1.260
	$O_2\cdots O_4$	2.803	2.764	2.780	2.784	2.772	2.759	2.759	2.772
angle (°)	$O_2-C_2-C_3$	125	124	128	128	125	124	128	127
	$O_2-C_2-C_1$	115	116	113	113	116	115	113	114
	$C_2-C_3-C_4$	124	124	121	119	123	123	120	121
	O_2-U-O_4	71	71	69	70	69	69	68	69
Mulliken charges (e)	U	2.330	1.534	2.331	1.570	2.357	1.561	2.344	1.574
	O_U	−0.498	−0.370	−0.458	−0.339	−0.506	−0.390	−0.472	−0.350
	UO_2	1.334	0.794	1.415	0.892	1.345	0.781	1.400	0.874
	S	0.064	0.092	0.069	0.120	0.079	0.109	0.100	0.142
	L	−0.699	−0.443	−0.742	−0.506	−0.712	−0.445	−0.750	−0.508
	O_2	−0.824	−0.569	−0.802	−0.555	−0.806	−0.555	−0.780	−0.539
	C_2	0.635	0.453	0.455	0.305	0.620	0.450	0.449	0.300
	C_3	−0.537	−0.314	−0.505	−0.297	−0.540	−0.309	−0.512	−0.300
	H_3	0.188	0.123	0.269	0.187	0.180	0.118	0.262	0.180
	C	−0.568	−0.529	1.297	0.886	−0.568	−0.529	1.296	0.805
	X	0.194	0.173	−0.401	−0.278	0.190	0.169	−0.405	−0.280
	CX_3	0.012	−0.009	0.091	+0.052	0.002	−0.022	+0.081	+0.041

[a] The ESP charges are given in Table S7.

TABLE 5: Free LH Ligands and Their UO_2L_2 and UO_2L_2S Complexes in Pure SC−CO_2 Solution[a]

solute	Elec	vdW	total
AAH diketone	−2.8 ± 1.9	−10.2 ± 1.7	−13.0 ± 2.8
FAHdiketone	−1.9 ± 1.4	−11.9 ± 1.8	−13.8 ± 2.4
AAH enol	−2.0 ± 1.8	−8.9 ± 1.4	−10.9 ± 2.1
FAH enol	−1.1 ± 1.5	−12.3 ±1.6	−13.4 ± 2.0
$UO_2(AA)_2$	−4.0 ± 2.4	−22.3 ± 2.6	26.3 ± 3.6
$UO_2(FA)_2$	−5.2 ± 3.3	−24.4 ± 2.5	−29.6 ± 3.2
$UO_2(AA)_2$(TBP)	−3.0 ± 3.5	−29.2 ± 2.7	−32.2 ± 4.2
$UO_2(FA)_2$(TBP)	−5.0 ± 3.6	−32.5 ± 3.7	−37.5 ± 5.5
$UO_2(AA)_2$ (H_2O)	−5.0 ± 3.1	−22.0 ± 2.9	−27.0 ± 4.5
$UO_2(FA)_2$ (H_2O)	−5.7 ± 3.7	−24.8 ± 2.9	−30.3 ± 4.5

[a] Average interaction energy with CO_2 and its components and fluctuations (kcal/mol). A full version of the Table is given in the Supporting Information (Table S5). The results of simulations with ESP charges are given in Table S8.

forms).[74,75] The $UO_2(FA)_2$ complex is similarly better solvated than $UO_2(AA)_2$ (−29.6 and −26.3 kcal/mol, respectively), due to both van der Waals (Δ = 2.1 kcal/mol) and electrostatic energy components (Δ = 1.2 kcal/mol).[76] As expected, the interaction with CO_2 increases with the number of ligands, i.e., from four to five-coordinated uranyl, and $UO_2(FA)_2$(TBP) interacts better than $UO_2(AA)_2$(TBP) with CO_2 (−37.5 versus −32.2 kcal/mol, respectively), due to the van der Waals (Δ = 3.3 kcal/mol) and the electrostatic energy contributions (Δ = 2.0 kcal/mol).[77] Further dissection of the complex into pieces shows that the larger contribution of the FA^- compared to the AA^- ligands (Δ = 5.0 kcal/mol) is mostly of van der Waals origin. This contrasts with what was observed with the $UO_2\mathbf{L}_2$ complexes.[76] As concerns the $UO_2\mathbf{L}_2(H_2O)$ complexes in which uranyl is also shielded from the CO_2 solvent, the F complex is again better solvated than the H complex (by 3.3 kcal/mol), and for a given diketonate ligand, the TBP adduct is better solvated than the H_2O adduct (by 6−7 kcal/mol).

These conclusions obtained with Mulliken charges on the complexes were confirmed by independent simulations performed with Merz−Kollman ESP charges on $UO_2\mathbf{L}_2$ and $UO_2\mathbf{L}_2$(TBP) complexes. The charges are given in Tables S6 and S7, and the resulting interaction energies with CO_2 are given in Table S8. With ESP charges, the F complexes are again better solvated than their H-analogues, by 4.8 kcal/mol for $UO_2\mathbf{L}_2$, and 6.0 kcal/mol for $UO_2\mathbf{L}_2$(TBP) complexes. This shows that the calculated higher CO_2-philicity of the F complexes is not critically dependent on the electrostatic representation of the solutes, due to the dominant van der Waals contributions.

III. β-Diketonates and Their Uranyl Complexes at the CO_2−Water Interface and the Synergistic Effect of TBP. In this section, we investigate the interfacial behavior of the free ligands in their neutral and deprotonated states, of tetracoordinated $UO_2\mathbf{L}_2$ and pentacoordinated $UO_2\mathbf{L}_2$(TBP) uranyl complexes,[73] comparing F versus H ligands. We want to investigate to which extent the complexes will be extracted to the CO_2 phase, or whether they adsorb at the interface. The simulations started with the solutes (ligands or uranyl complexes) near the interface, equally shared between the aqueous and CO_2 phases (see Figures 2 and 4). The MD results (final snapshots and average density curves of the solutes and solvents) reveal a marked effect of ligand fluorination, generally driving the system toward enhanced extraction.

Free LH Ligands. The free **L**H neutral ligands were simulated in their *cis*-enol form, as a 3*4*8 grid of 96 molecules at the interface (Figure 4). After 1 ns of dynamics, most of them (40% for the AAH ligands, and 35% for the FAH ones) sit in the CO_2 phase. In water, one finally finds 2 AAH, but no FAH ligand, which is consistent with the increased hydrophobicity upon fluorination. The remaining ligands sit at the interface. Interestingly, most of those that are the CO_2 phase retain their internal $OH\cdots O_L$ internal *cis*-hydrogen bond. This contrasts with the interfacial ligands whose enolic proton forms a trans $H_2O\cdots H-O_L$ hydrogen bond, while their other carbonyl oxygen is hydrogen bonded to another water molecule (Figure 5). The statistics over the last 0.6 ns for *all* ligands also gives a higher

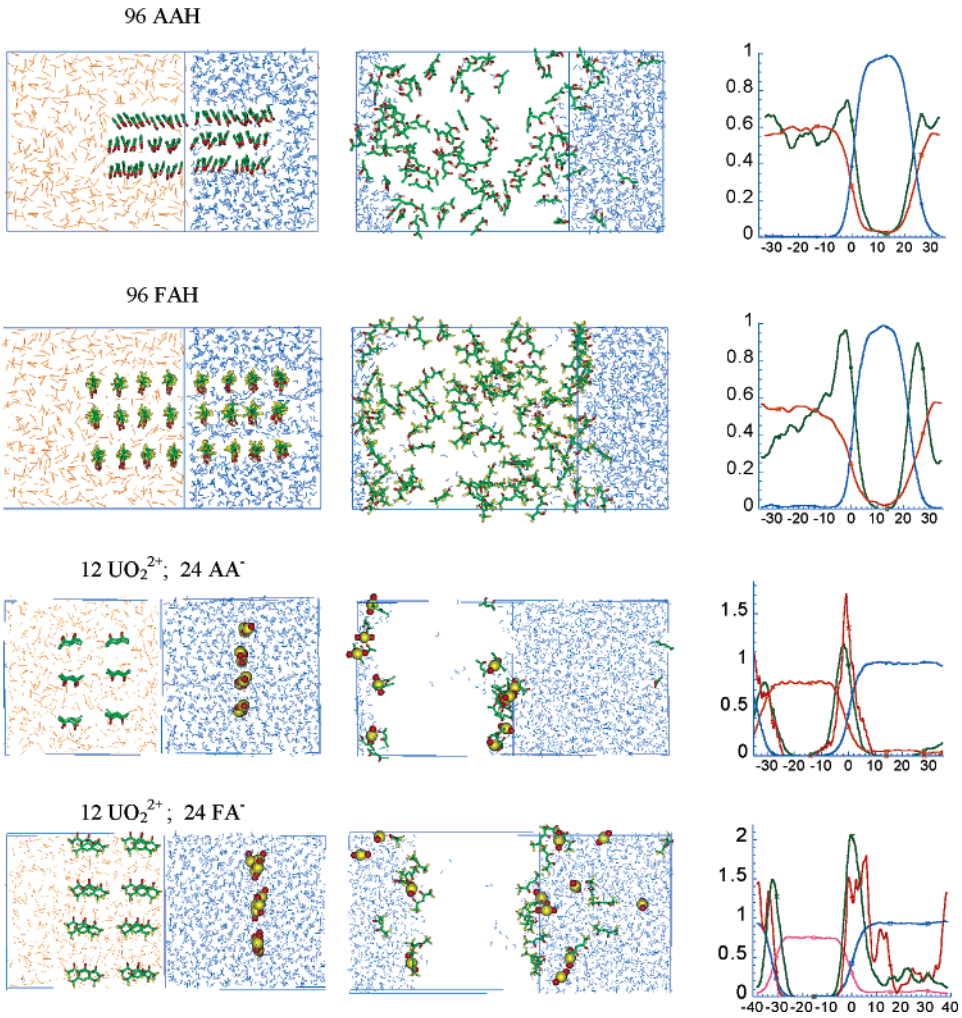

Figure 4. The neutral 96 **L**H-enols and "dissociated" uranyl diketonates (12 UO_2^{2+}, 2$\mathbf{L}^-$) at the CO_2−water interface. From left to right: snapshots of initial (0 ns) and final (1 ns) arrangements, and average density curves along the *z* axis (averages over the last 0.2 ns; color coded with water in blue, CO_2 in orange, ligands in green and uranyl in red).

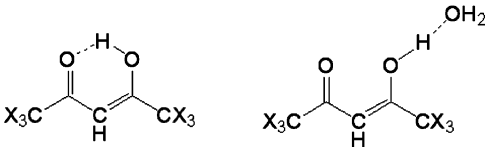

Figure 5. Schematic representation of internal versus intermolecular hydrogen bonds formed by the **L**H enols.

proportion of conformers with internal hydrogen bonds with AAH (76%) than with FAH (23%) enols, indicating that FAH enols display weaker internal hydrogen bonding than the AAH ones.[75] As a result, they interact better with water and are therefore more surface active and less concentrated in the CO_2 phase.

UO_2^{2+}, 2L^- "Dissociated" Ions. The uncomplexed ligands in their anionic forms AA^- and FA^- were simulated with UO_2^{2+} as counterions i.e., 12 [UO_2^{2+}, 2$\mathbf{L}^-$] species (see Figure 4). Initially, the UO_2^{2+} cations were on the aqueous side, while the most of the ligands were on the CO_2 side of the interface, well separated from the cations (at more than 20 Å). At the end of the dynamics, different final distributions are observed. Of particular interest is the *spontaneous complexation* of UO_2^{2+} by $\mathbf{L}^-$ ligands and the fact that this process is less important with the F ligands (one finds 1 labile $UO_2(FA)_2$ + 6 stable $UO_2(FA)^+$ complexes) than with the H ligands (8 $UO_2(AA)_2$ + 4 $UO_2(AA)^+$ complexes). Thus, with H ligands, all uranyl cations are complexed by at least on AA^- ligand, while with the F ligands only 7/12 of the cations are complexed. This is consistent with the reduction of carbonyl oxygen charge and basicity upon ligand fluorination, thus following the same trends as in the quantum mechanically optimized complexes. Looking at the stoichiometry of the complexes, one also finds less $UO_2\mathbf{L}_2$ than $UO_2\mathbf{L}^+$ species after ligand fluorination. Fluorination also modifies the interfacial landscape. All $UO_2\mathbf{L}_2$ and $UO_2\mathbf{L}^+$ complexes sit at the interface, where they achieve a five equatorial coordination by co-complexing 1 and 3 H_2O molecules, respectively (Figure 6). Some $UO_2(AA)(H_2O)_3^+$ complexes make excursions to the CO_2 phase and come back to the interface. They are thus too hydrophilic to be extracted. Most of the remaining free $\mathbf{L}^-$ ligands sit at the interface, where their number increases (from 3 to 16) upon fluorination. As a result, with the H ligands, the aqueous phase contains only one AA^- ligand and no free UO_2^{2+} ion, whereas with F ligands, it contains 5 penta-hydrated $UO_2(H_2O)_5^{2+}$ ions plus 5 FA^- anions, presumably attracted by the uranyls. This series of simulations highlight the effect of ligand fluorination but may not correspond to a realistic model for experiments starting, e.g. with free **L**H ligands in CO_2 and uranyl salts (e.g. $UO_2(NO_3)_2$) in water, and involve proton transfer and complexation reactions.

UO_2L_2 and UO_2L_2(TBP) Complexes. Because classical MD simulations can hardly describe bond making or breaking processes, we decided to simulate next the $UO_2\mathbf{L}_2$ and $UO_2\mathbf{L}_2$(TBP) complexes, starting with a grid of 2*6 solutes. This led

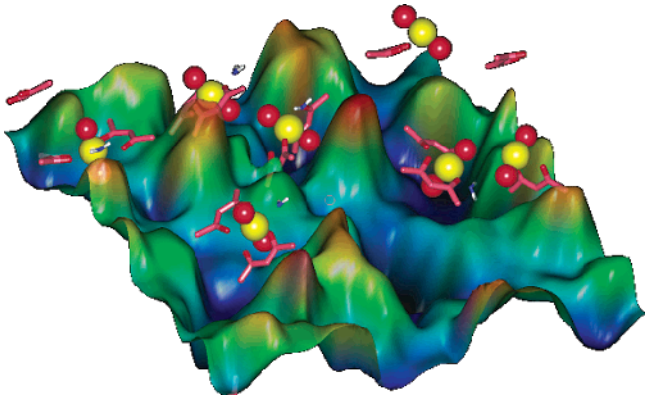

Figure 6. Spontaneous formation of $UO_2(AA)_2(H_2O)$ complexes at the CO_2-water interface in the simulation which started with dissociated uranyl diketonate salts (12 UO_2^{2+}, 2 $\mathbf{L}^-$) (see Figure 4). Water (on the topside of the interface) and CO_2 (on the bottom side on the interface) not represented for clarity.

to major reorganization and to different final arrangements (Figure 7). Most of the F- and H-unsaturated $UO_2\mathbf{L}_2$ complexes captured an H_2O molecule to form $UO_2\mathbf{L}_2(H_2O)$ species. None of these are found in the CO_2 phase. The majority (92%, on the average for the $UO_2(AA)_2(H_2O)$ complexes and 85% for the $UO_2(FA)_2(H_2O)$ complexes) adsorbed at one interface, whereas the remaining ones sit in the "bulk" CO_2 phase. Notice the higher proportion of "extracted" complexes with the F than with the H ligands. The higher hydrophobicity of the former ones can also be seen from the fact that they sit on the CO_2 side of the interface, whereas the $UO_2(AA)_2$ complexes sit on the water side.

Upon coordination of one "synergistic" TBP ligand, the $UO_2\mathbf{L}_2$ complexes become more hydrophobic and less surface active, as seen from the lower proportion of complexes at the interface: 71% for $UO_2(AA)_2$(TBP) and 32% for $UO_2(FA)_2$-(TBP) complexes. None of them finally sit in water, and the most remarkable result concerns the higher extraction of F complexes (68%), compared to the H ones (29%). This is fully consistent with experimental trends and, when compared to the unsaturated $UO_2\mathbf{L}_2$ complexes, demonstrates the role of TBP which shields uranyl from the solvent and makes the complexes more hydrophobic and CO_2-philic.[78] Figure 8 represents a snapshot of the water surface in contact with CO_2, showing UO_2-$(AA)_2$(TBP) complexes weakly adsorbed on the CO_2 side of the interface, in equilibrium with "extracted" complexes. It can be seen that the surface is very rough (see also Figure 6). The *z*-extrema are about 13 Å apart and exchange dynamically.

UO_2L_2(TBP) Complexes with an Excess of TBP. The simulation of the systems of 12 $UO_2\mathbf{L}_2$(TBP) complexes with H versus F ligands in the presence of TBP in excess (60 TBP molecules) reveals another important effect of TBP as synergistic agent (see Figure 9). The dynamics started with a "symmetrical" distribution of the solutes on the two sides of the interface but,

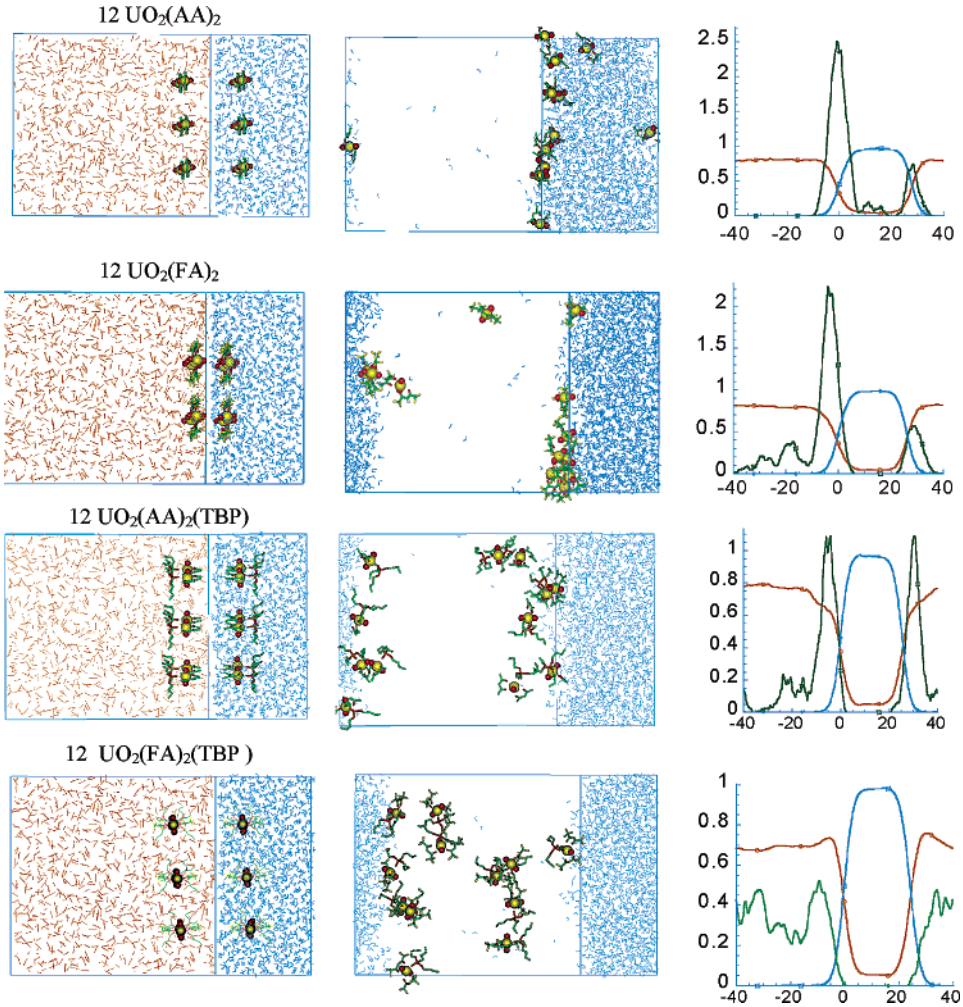

Figure 7. Twelve $UO_2\mathbf{L}_2$ and $UO_2\mathbf{L}_2$(TBP) complexes at the CO_2−water interface. From left to right: snapshots of initial (0 ns) and final (1.5 ns) arrangements, and average density curves along the *z* axis (averages over the last 0.2 ns; color coded with water in blue, CO_2 in orange, uranyl in green).

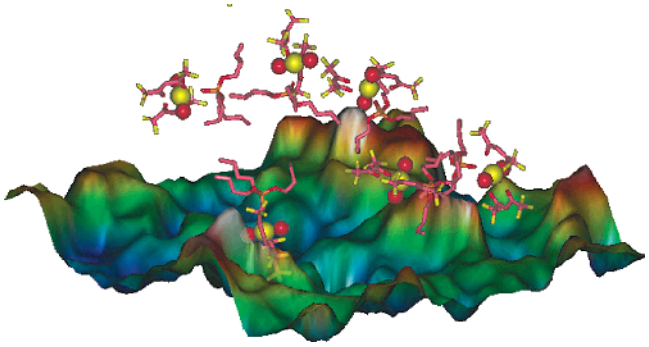

Figure 8. Snapshot of the CO_2 side of the interface with $UO_2(FA)_2$-(TBP) complexes. Water (on the bottom side of the interface) and CO_2 (on the top side on the interface) not represented for clarity.

after 2 ns, all TBPs and complexes which were in water migrated to the two interfaces or to CO_2. The majority of complexes (90% with F ligands and 80% with H ligands) were extracted to CO_2, while the remaining ones adsorbed at the interface.[79] Thus, when compared to the system without TBP in excess, these simulations reveal the importance of TBP concentration to extract the $UO_2\mathbf{L}_2$(TBP) complexes to CO_2 and confirm that there is more extraction with the F than with the H ligands. The reason can be found in the higher surface activity of TBP (65% and 70%, respectively, adsorb at the interface), compared to the uranyl complexes (10% and 20%, respectively), related to hydrogen bonding interactions of interfacial water with TBP. At the interface, the TBPs form an irregular diluted "layer", which is more favorable for liquid−liquid extraction than a regular monolayer ("film") which would be deleterious.

Discussion and Conclusion

We present theoretical investigations on the effect of fluorination of an important class of ligands that are used to complex and extract *f* elements to SC−CO_2, combining two approaches: QM calculations allowed us to investigate the complexation energy and acidity of the ligands in the gas phase and MD simulations to investigate the solvation and interfacial behavior of the F/H ligands and complexes. They provide complementary and converging views on the effect of ligand fluorination, and on the synergistic effect of TBP in supercritical fluid extraction. First, uranyl intrinsically prefers to complex a fluorinated FAH ligand than its AAH analogue. This is because the increase in acidity upon fluorination overcompensates the weaker coordination of the fluorinated β-diketonate anions. This effect is observed with unsaturated $UO_2\mathbf{L}_2$, as well as with five-coordinated $UO_2\mathbf{L}_2S$ complexes (S = TMP or H_2O). Intrinsically, also, the $UO_2\mathbf{L}_2$ complexes display a higher affinity for phosphoryl-containing ligands such as TMP or TBP than for H_2O, following the relative Lewis acidities of these oxygen donors. This is a first important role of synergistic TBP which prevents hydration of the uranyl complex and enhances its CO_2-philic character. This is consistent with the experimental solubility of $Cu(FA)_2$ in SC−CO_2 which drops from $3.21\cdot10^{-3}$ to $1.74\cdot10^{-3}$ mole.l^{-1} upon coordination of one H_2O molecule to the metal at 313 K.[1] Conversely, it has been observed that the formation of lanthanide and uranium fluorinated β-diketonate adducts with phosphoryl-containing Lewis bases S greatly improves their solubility in SC−CO_2, and that the sequence of stabilities follows the order S = TOPO (trioctyl phosphine oxide) > TBPO (tributyl phosphine oxide) > TBP,[11] i.e., the order of oxygen basicity. This is fully consistent with our results on H_2O versus TBP (TMP) ligands. Furthermore, according to our calculations, the F-diketonates display a stronger affinity than H-diketonates for a given S ligand.

MD simulations in an explicitly represented CO_2 solution show that the F ligands and their $UO_2(FA)_2$ and $UO_2(FA)_2S$ complexes are better solvated than their H analogues are. The analysis of solute−solvent interaction energies also makes clear that the complexes with TBP are better solvated by CO_2 than those with H_2O, following experimental trends. This is also consistent with the high solubility of TBP in CO_2, which contrasts with the corresponding low water solubility.[80] The simulation results in CO_2 solution allow us to better understand the trends observed at the CO_2−water interface. Not surprisingly, the free ligands **L**H in their *cis*-enol form are surface active, due to their amphiphilic structure: the polar carbonyl and hydroxyl moieties are attracted by water, while the (F)-alkyl groups prefer the CO_2 environment. The $UO_2\mathbf{L}_2$ diketonate complexes are unsaturated and capture a water molecule during the dynamics, leading to the adsorption of a majority of complexes at the interface, in equilibrium with a few extracted ones whose proportion increases upon ligand fluorination. The

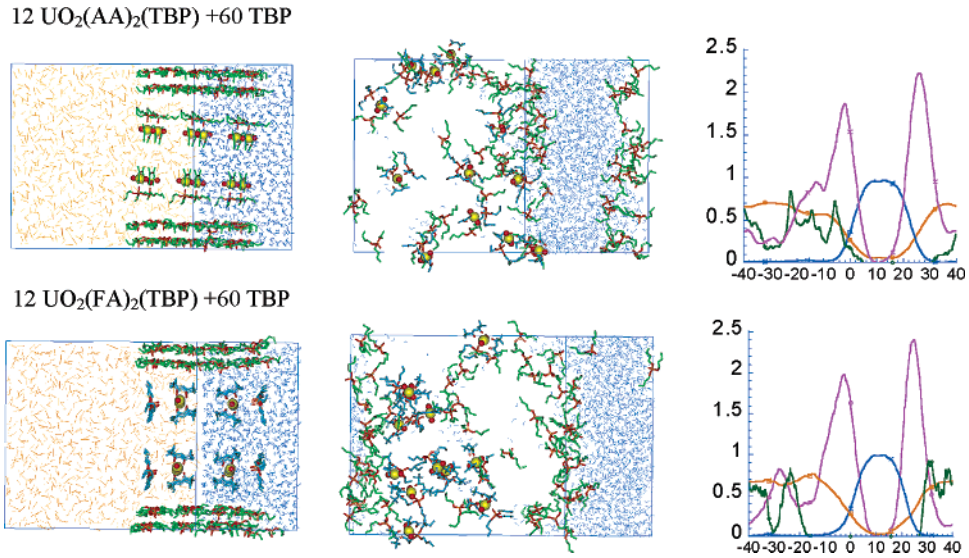

Figure 9. 12 $UO_2\mathbf{L}_2$(TBP) complexes + 60 TBPs at the CO_2−water interface. From left to right: snapshots of initial (0 ns) and final (1.5 ns) arrangements, and average density curves along the *z* axis (averages over the last 0.2 ns; color coded with water in blue, CO_2 in orange, complexes in green, free TBP in purple).

most interesting case concerns the $UO_2\mathbf{L}_2$(TBP) complexes which are more hydrophobic and CO_2-philic than the $UO_2\mathbf{L}_2$-(H_2O) analogues and, again, the highest extraction is observed with the fluorinated diketonate ligands. In the presence of an excess of TBP molecules, which preferentially adsorb at the interface, all uranyl complexes with F ligands are extracted, which points to another important role of synergistic ligands. These are generally surface active and lower the interfacial pressure between the aqueous and supercritical phases, thus facilitating the transfer of the complexed metals to SC−CO_2. We notice that solvent modifiers such as alcohols, also known to promote the supercritical fluid extraction of metals,[1,4] may play, like TBP, a dual synergistic role: (i) co-complexation of the metal with the "main ligands" (e.g., diketonates and phosphoric or dithiophosphinic acid derivatives), leading to hydrophobic complexes suitable to partition to the "oil" phase, and (ii) modification of the water−"oil" interface properties, facilitating the migration of the complex through the interface. "Interface" not only refers to a "planar" interface between the two phases but may involve the surface of micelles or microdroplets.[81] The evolution from well-defined interfaces to cylindrical or spherical micelles, as well as the condensation of droplets also reduces the interfacial area, hence inducing the migration of the interfacial ligands and complexes toward the supercritical or "oil" phases.

Acknowledgment. The authors are grateful to IDRIS, CINES, and Université Louis Pasteur for computer resources and to E. Engler for assistance. N.G. thanks the French Ministry of Research for a grant.

Supporting Information Available: Table S1: Total energies (in a. u.) of the QM optimized ligands and complexes. Table S2: Main structural and electronic features of the **L**H enols. Table S3: Main structural and electronic features of the $\mathbf{L}^-$ diketonates (cis form). Table S4: Main structural and electronic features of the $\mathbf{L}^-$ diketonates (trans form). Table S5: Free **L**H ligands and their $UO_2\mathbf{L}_2$ and $UO_2\mathbf{L}_2$S complexes in pure SC−CO_2 solution: average interaction energy with CO_2 and its components, and fluctuations (kcal/mol). Table S6: ESP Charges from DFT//DFT calculations of $\mathbf{UO_2L_2}$ complexes. Table S7: ESP charges from DFT//DFT calculations of $\mathbf{UO_2L_2}$-(**TMP**) complexes (S = TMP). Table S8: $UO_2\mathbf{L}_2$ and $UO_2\mathbf{L}_2$-TMP complexes modeled with ESP charges (DFT//DFT calculations), in pure SC−CO_2 solution: average interaction energy with CO_2 and its components, and fluctuations (kcal/mol). Table S9: $UO_2\mathbf{L}_2$ and $UO_2\mathbf{L}_2$S complexes at the CO_2 water interface: average interaction energy between one complex and CO_2 or water, and fluctuations (kcal/mol). Figure S1: AMBER atom types and atomic charges (ESP charges for the **L**H and $\mathbf{L}^-$ free ligands and Mulliken charges for the complexes). ESP charges of the uranyl complexes are given in Tables S6 and S7. This material is available free of charge via the Internet at http://pubs.acs.org.

References and Notes

(1) Erkey, C. *J. Supercrit. Fl.* **2000**, *17*, 259−287.
(2) Laintz, K. E.; Wai, C. M.; Yonker, C. R.; Smith, R. D. *J. Supercrit. Fluids* **1991**, *4*, 194−198.
(3) Laintz, K. E.; Wai, C. M.; Yonker, C. R.; Smith, R. D. *Anal. Chem.* **1992**, *64*, 2875.
(4) Wai, C. M.; Wang, S. *J. Chromatogr. A* **1997**, *785*, 369−383.
(5) Smart, N. G.; Carleson, T.; Kast, T.; Clifford, A. A.; Burford, M. D.; Wai, C. M. *Talanta* **1997**, *44*, 137−150.
(6) Lin, Y.; Smart, N. G. In *Supercritical Carbon Dioxide*; Gopalan, A. S., Wai, C. M., Jacobs, H. K., Eds.; American Chemical Society: Washington, DC, 2003; pp 23−35.
(7) Ashraf-Khorassani, M.; Combs, M. T.; Taylor, L. T. *J. Chromatogr. A* **1997**, *774*, 37−49.
(8) Tingey, J. M.; Yonker, C. R.; Smith, R. D. *J. Phys. Chem.* **1989**, *93*, 2140.
(9) Lin, Y.; Brauer, R. D.; Laintz, K. E.; Wai, C. M. *Anal. Chem.* **1993**, *65*, 2549−2551.
(10) Lin, Y.; Wai, C. M.; Jean, F. M.; Brauer, R. D. *Environ. Sci. Technol.* **1994**, *28*, 1190−1193.
(11) Lin, Y.; Wu, H.; Smart, N. G.; Wai, C. M. *J. Chromatography A* **1998**, *793*, 107−113.
(12) Shadrin, A.; Mursin, A.; Romanovskii, V. Extraction Processes in XXI Century. *Proc. of Int. Symp.* **1999**, 246−255.
(13) Lin, Y.; Wu, H.; Wai, C. M.; Smart, N. G. *Talanta* **2000**, 23−35.
(14) Schurhammer, R.; Berny, F.; Wipff, G. *Phys. Chem. Chem. Phys.* **2001**, *3*, 647−656.
(15) Schurhammer, R.; Wipff, G. *New J. Chem.* **2002**, *26*, 229−233.
(16) Schurhammer, R.; Wipff, G. In *Separations and Processes Using Supercritical Carbon Dioxide*; Gopalan, A. S.; Wai, C.; Jacobs, H. Ed.; American Chemical Society: Washington, DC, 2003; pp 223−244.
(17) Vayssière, P.; Wipff, G. *Phys. Chem. Chem. Phys.* **2003**, *5*, 127−135.
(18) Vayssière, P.; Wipff, G. *Phys. Chem. Chem. Phys.* **2003**, *5*, 2842−2850.
(19) Szymanowski, J. *Solv. Extract. Ion Exch.* **2000**, *18*, 729−751.
(20) Frisch, M. J.; Trucks, G. W.; Schlegel, H. B.; Scuseria, G. E.; Robb, M. A.; Cheeseman, J. R.; Zakrzewski, V. G.; Montgomery, J. A., Jr.; Stratmann, R. E.; Burant, J. C.; Dapprich, S.; Millam, J. M.; Daniels, A. D.; Kudin, K. N.; Strain, M. C.; Farkas, O.; Tomasi, J.; Barone, V.; Cossi, M.; Cammi, R.; Mennucci, B.; Pomelli, C.; Adamo, C.; Clifford, S.; Ochterski, J.; Petersson, G. A.; Ayala, P. Y.; Cui, Q.; Morokuma, K.; Malick, D. K.; Rabuck, A. D.; Raghavachari, K.; Foresman, J. B.; Cioslowski, J.; Ortiz, J. V.; Stefanov, B. B.; Liu, G.; Liashenko, A.; Piskorz, P.; Komaromi, I.; Gomperts, R.; Martin, R. L.; Fox, D. J.; Keith, T.; Al-Laham, M. A.; Peng, C. Y.; Nanayakkara, A.; Gonzalez, C.; Challacombe, M.; Gill, P. M. W.; Johnson, B. G.; Chen, W.; Wong, M. W.; Andres, J. L.; Head-Gordon, M.; Replogle, E. S.; Pople, J. A. *Gaussian 98*, revision A.5; Gaussian, Inc.: Pittsburgh, PA, 1998.
(21) Ortiz, J. V.; Hay, P. J.; Martin, R. L. *J. Am. Chem. Soc.* **1992**, *114*, 2736−2737 and references therein.
(22) Hutschka, F.; Troxler, L.; Dedieu, A.; Wipff, G. *J. Phys. Chem. A* **1998**, *102*, 3773−3781.
(23) Sémon, L.; Boehme, C.; Billard, I.; Hennig, C.; Lützenkirchen, K.; Reich, T.; Rossberg, A.; Rossini, I.; Wipff, G. *ChemPhysChem* **2001**, *2*, 591−598.
(24) Spencer, S.; Gagliardi, K.; Handy, N. C.; Ioannou, A. G.; Skylaris, C.-K.; Willetts, A.; Simper, A. M. *J. Phys. Chem. A* **1999**, *103*, 1831−1837.
(25) Schreckenbach, G.; Hay, P. J.; Martin, R. L. *J. Comput. Chem.* **1999**, *20*, 70−90.
(26) Vasquez, J.; Bo, C.; Poblet, J. M.; Pablo, J. d.; Bruno, J. *Inorg. Chem.* **2003**, *42*, 6136−6141.
(27) Clavaguera-Sarrio, C.; Brenner, V.; Hoyau, S.; Marsden, C. J.; Millié, P.; Dognon, J.-P. *J. Phys. Chem. B* **2003**, *107*, 3051−3060.
(28) Brynda, M.; Wesolowski, T. A.; Wojciechowski, K. *J. Phys. Chem. A* **2004**, *108*, 5091−5099.
(29) Vallet, V.; Wahlgren, U.; Schimmelfpennig, B.; Szabo, Z.; Grenthe, I. *J. Am. Chem. Soc.* **2001**, *123*, 11999−12008.
(30) Vallet, V.; Moll, H.; Wahlgren, U.; Szabo, Z.; Grenthe, I. *Inorg. Chem.* **2003**, *42*, 1982−1993.
(31) Wahlgren, U.; Moll, H.; Grenthe, I.; Schimmelfpennig, B.; Maron, L.; Vallet, V.; Gropen, O. *J. Phys. Chem. A* **1999**, *103*, 8257−8264.
(32) Gagliardi, K.; Grenthe, I.; Roos, B. *Inorg. Chem.* **2001**, *40*, 2976−2978.
(33) Kaltsoyannis, N. *Chem. Soc. Rev.* **2003**, *32*, 9−16.
(34) Küchle, W.; Dolg, M.; Stoll, H.; Preuss, H. *J. Chem. Phys.* **1994**, *100*, 7535−7542.
(35) Institut für Theoretische Chemie, Universität Stuttgart. ECPs and corresponding valence basis sets. http://www.theochem.uni-stutgart.de.
(36) Coupez, B.; Wipff, G. *Inorg. Chem.* **2003**, *42*, 3693−3703.
(37) Boys, S. F.; Bernardi, F. *Mol. Phys.* **1970**, *19*, 553−566.
(38) Case, D. A.; Pearlman, D. A.; Caldwell, J. W.; Cheatham III, T. E.; Wang, J.; Ross, W. S.; Simmerling, C. L.; Darden, T. A.; Merz, K. M.; Stanton, R. V.; Cheng, A. L.; Vincent, J. J.; Crowley, M.; Tsui, V.; Gohlke, H.; Radmer, R. J.; Duan, Y.; Pitera, J.; Massova, I.; Seibel, G. L.; Singh, U. C.; Weiner, P. K.; Kollman, P. A. *AMBER7*; University of California: San Francisco 2002.
(39) See for instance the ESP charges of the Nitrogen atom of NMe_4^+ which are positive, i.e., opposite to expected trends based on electronegativities, while the Mulliken charges are negative (Luzkhov, V.; et al. *Phys. Chem. Chem. Phys.* **2002**, *4*, 4640−4647).
(40) Guilbaud, P.; Wipff, G. *J. Mol. Struct. (THEOCHEM)* **1996**, *366*, 55−63.

(41) Gough, C. A.; DeBolt, S. E.; Kollman, P. A. *J. Comput. Chem.* **1992**, *13*, 963−970.
(42) Murthy, C. S.; Singer, K.; McDonald, I. R. *Mol. Phys.* **1981**, *44*, 135−143.
(43) Jorgensen, W. L.; Chandrasekhar, J.; Madura, J. D.; Impey, R. W.; Klein, M. L. *J. Chem. Phys.* **1983**, *79*, 926−936.
(44) Cornell, W. D.; Cieplak, P.; Bayly, C. I.; Gould, I. R.; Merz, K. M.; Ferguson, D. M.; Spellmeyer, D. C.; Fox, T.; Caldwell, J. W.; Kollman, P. A. *J. Am. Chem. Soc.* **1995**, *117*, 5179−5197.
(45) Darden, T. A.; York, D. M.; Pedersen, L. G. *J. Chem. Phys.* **1993**, *98*, 10089.
(46) Graham, B. F.; Lagalante, A. F.; Bruno, T. J.; Harrowfield, J. M.; Trengove, R. D. *Fluid Phase Equilib.* **1998**, *150*−*151*, 829−838.
(47) Berendsen, H. J. C.; Postma, J. P. M.; van Gunsteren, W. F.; DiNola, A. *J. Chem. Phys.* **1984**, *81*, 3684−3690.
(48) Tironi, I. G.; Sperb, R.; Smith, P. E.; van Gunsteren, W. F. *J. Chem. Phys.* **1995**, *102*, 5451−5459.
(49) Emsley, J. *Struct. Bond., Berlin* **1984**, *57*, 147−191.
(50) Lowrey, A. H.; D'Antonio, C. G. P.; Karle, J. *J. Am. Chem. Soc.* **1971**, *93*, 6399−6404.
(51) Andreassen, A. L.; Bauer, S. H. *J. Mol. Struct.* **1972**, *12*, 381−403.
(52) Ijima, K.; Ohnogi, A.; Shibata, S. *J. Mol. Struct.* **1987**, *156*, 111−118.
(53) Andreassen, A. L.; Zebelman, D.; Bauer, S. H. *J. Am. Chem. Soc.* **1971**, *93*, 1148−1152.
(54) Funck, E.; Mecke, R. In *Hydrogen Bonding*; Hadzi, D., Ed.; Pergamon Press: London, 1959; pp p 433.
(55) Dannenberg, J. J.; Rios, R. *J. Phys. Chem.* **1994**, *98*, 6714−6718.
(56) Boese, R.; Antipin, M. Y.; Bläser, D.; Lyssenko, K. A. *J. Phys. Chem. B* **1998**, *102*, 8654−8660.
(57) Gilli, P.; Belluci, F.; Ferretti, V.; Bertolasi, V. *J. Am. Chem. Soc.* **1989**, *111*, 1023−1028.
(58) Sliznev, V. V.; Lapshina, S. B.; Girichev, G. V. *J. Struct. Chem.* **2002**, *43*, 47−55.
(59) Wallen, S. P.; Yonker, C. R.; Phelps, C.; Wai, C. M. *Faraday Trans.* **1997**, *93*, 116.
(60) The preference of AA^- for the trans form is likely due to internal hydrogen bonding C═O···H_3C attractions and to avoided carbonyl-carbonyl repulsions of the cis form. In the FA^- anion, these are less important (due to carbonyl charge dilution into the CF_3 groups), whereas the trans form is somewhat destabilized by a carbonyl···CF_3 repulsion.
(61) Noro, J.; Sekine, T. *Bull. Chem. Soc. Jpn.* **1993**, *66*, 1647.
(62) McMahon, T. B.; Kebarle, P. *J. Am. Chem. Soc.* **1976**, *98*, 3399−3406.
(63) Lin, Y.; Smart, N. G.; Wai, C. M. *Environ. Sci. Technol.* **1995**, *29*, 2706−2708.
(64) Phelps, C. L.; Smart, N. G.; Wai, C. M. *J. Chem. Educ.* **1997**, *73*, 1163−1168.
(65) Allen, F. H.; Kennard, O. *Chem. Des. Automat. News* **1993**, *8*, 31−37.
(66) Frasson, E.; Bombieri, G.; Panattoni, C. *Coord. Chem. Rev.* **1966**, *1*, 145.
(67) Taylor, J. C.; Waugh, A. B. *J. Chem. Soc., Dalton Trans.* **1977**, 1630.
(68) See the REFCODES of structures of UO_2(diketonate)$_2$S complexes with S = H_2O (ACACUO10), carbonyl (ACAPOU, ACAPUR, ACDXUS, TULFEL, XACPAU), phosphoryl (ACPOXU, HFPOPU, HFPOPU01, TFOPOU, XICWOV), alcohol (BIHCOK), pyridine (CEMGUW, FORKEC, FORKIG), NH_3 (HFAPAU), NO_3^- (PPNXUA) ligands in the Cambridge Crystallographic Structural Database.
(69) Batzar, K.; Goldberg, D. E.; Newman, L. *J. Inorg. Nucl. Chem.* **1967**, *29*, 1511.
(70) Lin, Y.; Smart, N. G.; Wai, C. M. *Trends Anal. Chem* **1995**, *14*, 123.
(71) Gutman, V., Ed.; *The Donor*−*Acceptor Approach to Molecular Interactions*; Plenum Press: New York, 1980.
(72) This compensation effect is consistent with theoretical calculations on M**L**$_3$(TOPO) complexes (**L**$^-$ = tropolonate bidentate anion $C_7H_5O_2^-$) with M^{3+} metals of increasing size and hardness. See: Narbutt, J.; Czerwinski, M.; Krejzler, J. *Eur. J. Inorg. Chem.* **2001**, 3187.
(73) The UO_2**L**$_2$ and UO_2**L**$_2$S complexes were simulated with U−O distances constrained to their AMBER energy minimized values in vacuo (with a force constant of 10 kcal/mol.Å^{-2}). To prevent large out-of-plane oscillations of equatorial ligands, the latter were also constrained to remain equatorial, therefore reducing the solvent accessibility to the U atom.
(74) Note that the enhanced interaction energy with the CO_2 solvent upon fluorination is larger for enols (2.5 kcal/mol) than for diketones (0.8 kcal/mol). This is because the FAH enol displays an equilibrium between cis and trans forms (see Figure 5) and the latter is stabilized by O−H··· O═C═O interactions. The AAH enol is cis and cannot display such interactions.
(75) The energy preference for the *cis*-enol (internal hydrogen bond) compared to the *trans*-enol is larger for the AAH ligands than for the FAH ligands: by 17.0 vs 10.1 kcal/mol (HF/6-31G* calculations), 17.1 vs 11.8 kcal/mol (DFT-B3LYP/6-31G* calculations), and 19.0 vs 12.5 kcal/mol (AMBER calculations). Note the good agreement between QM and AMBER results.
(76) The better solvation of the $UO_2(FA)_2$ complex, compared to $UO_2(AA)_2$ is not due to the ligand, but to the uranyl contribution. This is because O_{CO2} oxygens are attracted by the U_{UO2} atom in such a way to achieve a five-coordination for uranyl, and this is more pronounced in the F− than in the H complex, following the same trends as with H_2O or TMP ligands. The CO_2 molecule(s) coordinated to uranyl display instead repulsive electrostatic interactions with the F ligands. These AMBER results are confirmed by QM calculations on the CO_2 complexation by the UO_2L_2 complexes. CO_2 binds more strongly to $UO_2(FA)_2$ than to $UO_2(AA)_2$ (−8.2 and −5.6 kcal/mol, respectively at the HF level; −13.1 and − 8.7 kcal/mol respectively at the DFT level).
(77) A similar preference for the F complex is found when the simulations are run without constraints on the equatorial ligands to retain a planar coordination.
(78) The CO_2 phase displays attractive interactions with the complexes (Table S9). Averaging over all complexes shows that, after ligand fluorination, the attraction energy per UO_2**L**$_2$(TBP) complex with CO_2 increases from −26 to −31 kcal/mol, while the attraction with water drops from −21 to −4 kcal/mol, on the average. When compared to the corresponding unsaturated UO_2**L**$_2$ complexes, the TBP adducts are less attracted by water ($\Delta \approx 20$ kcal/mol), but are more attracted by CO_2 ($\Delta \approx$ 15 kcal/mol). These numbers thus translate both intrinsic trends, as well as the differences in distributions near the interface.
(79) These arrangements are mirrored by the energy component analysis with the $UO_2(AA)_2$(TBP) and $UO_2(FA)_2$(TBP) complexes (Table S9). Upon fluorination, the interaction energy with water decreases (from −10 kcal/mol to − 2 kcal/mol per complex on the average), whereas the interaction energy with CO_2 increases (from −28 to −33 kcal/mol). We notice that the interaction of one complex with the CO_2 phase is somewhat stronger when the TBPs are in excess (−28 and −33 ± 1 kcal/mol, respectively) than without TBP (−26 and −31 kcal/mol, respectively). These are smaller at the interface than in pure SC−CO_2 solution (−32 and −37 kcal/mol, respectively).
(80) Marcus, Y. *The Properties of Solvents*; Wiley Series in Solution Chemistry; John Wiley & Sons: Chichester, U.K., 1998.
(81) Coupez, B.; Boehme, C.; Wipff, G. *J. Phys. Chem. B* **2003**, *107*, 9484−9490.